Heliyon 7 (2021) e05866

Contents lists available at ScienceDirect

Heliyon

journal homepage: www.cell.com/heliyon

Research article

Optimization of the adsorption of total organic carbon from produced water using functionalized multi-walled carbon nanotubes

T.L. Adewoye [a,e,*], O.O. Ogunleye [b], A.S. Abdulkareem [c,e], T.O. Salawudeen [b], J.O. Tijani [d,e]

[a] Department of Chemical Engineering, University of Ilorin, PMB 1515 Ilorin, Kwara State, Nigeria
[b] Department of Chemical Engineering, Ladoke Akintola University of Technology, PMB 4000, Ogbomoso, Oyo State, Nigeria
[c] Department of Chemical Engineering, Federal University of Technology, PMB 65 Minna, Niger State, Nigeria
[d] Department of Chemistry, Federal University of Technology, PMB 65 Minna, Niger State, Nigeria
[e] Nanotechnology Research Group, Africa Centre of Excellence for Mycotoxin & Food Safety, Federal University of Technology, PMB 65 Minna, Niger State, Nigeria

ARTICLE INFO

Keywords:
Nano-adsorbent
CVD
MWCNTs
TOC
Adsorption
Produced water
Optimization

ABSTRACT

This study investigated the removal of Total Organic Carbon (TOC) from produced water by batch adsorption process using adsorbents developed from Multi-Walled Carbon Nanotubes (MWCNTs). The MWCNTs, synthesized by catalytic chemical vapour deposition method using kaolin-supported tri-metallic (iron-cobalt-nickel) catalyst were purified by H_2SO_4/HNO_3 and then functionalized with 1-pyrenebutanoic acid N-hydroxyl succinimidyl ester (PSE). The raw, purified and functionalized MWCNTs were characterized by High Resolution Scanning Electron Microscopy (HRSEM), High Resolution Transmission Electron Microscopy (HRTEM), Brunauer–Emmett-Teller (BET) and Fourier Transform Infrared Spectroscopy (FTIR). In the results, HRSEM/HRTEM revealed the structure, purity and also confirmed the attachment of the PSE molecule onto the nano-adsorbent(s). The BET surface areas of MWCNTs, PMWCNTs and FMWCNTs were 970.17, 869.25 and 831.80 m^2/g, respectively while the FTIR established the existence of surface functional groups. The functionalized MWCNTs (FMWCNTs) nano-adsorbent showed superior performance efficiency (93.6%) than the purified MWCNTs (PMWCNTs) (79.2%) as examined under the same batch adsorption condition: 0.02 g adsorbent dosage, 10–90 min contact time and 30 °C solution temperature probably, due the improved wettability resulted from incorporation of PSE. Subsequently, Central Composite Design (CCD) was applied to optimize the process parameters for the sorption of TOC onto FMWCNTs. The CCD in the response surface methodology predicted 260 mg/g adsorption capacity of FMWCNTs in the removal of TOC at the optimum condition of 49.70 min contact time, 34.81 °C solution temperature, and 0.02 g adsorbent dosage. The kinetics data were best described by pseudo-second-order model and thermodynamic parameters suggested that the process was feasible, spontaneous and exothermic. It can be inferred from the various analysis conducted that the developed FMWCNTs nano-adsorbent is effective for removal of TOC from oil-produced water and may be explored for removal of organic contaminants from other industrial wastewater.

1. Introduction

Nigeria is a country endowed with abundant crude oil resources and the revenue accrued from it has become the main stake of her economy [1]. However, continuous petroleum exploration activities in Nigeria especially in the Niger Delta area have resulted in unprecedented land and water pollution as a result of both accidental and indiscriminate discharge of crude oil and its associates [2, 3]. These discharges may be in form of leakages from pipelines, oil wells, underground storage tanks of a gas station, improper disposal of petroleum waste, sabotage, oil bunkering, and accidental spill from ruptured pipelines [4, 5]. One prominent derived waste from crude oil exploration is the produced water, which constitutes the largest volume of the waste stream in the oil and gas industries [6]. Approximately, nine barrels (378 gallons) of produced water is estimated by the American Petroleum Institute as being recovered for each barrel of oil in stripper oil well operations [7]. Produced water consists of a complex mixture of dissolved salts, hydrocarbons, heavy metals, organic and inorganic components, naturally occurring radioactive materials and added chemicals used in oil extraction and separation, potentially toxic elements, making it difficult to discard without some form of treatment [8].

* Corresponding author.
E-mail address: adewoye.tl@unilorin.edu.ng (T.L. Adewoye).

https://doi.org/10.1016/j.heliyon.2020.e05866
Received 21 July 2020; Received in revised form 23 October 2020; Accepted 23 December 2020

Several organic and inorganic components present in produced water can be potentially or more hazardous than the crude oil itself [9]. Organic pollutants can destruct the environment and constitute a health risk to man and the ecosystem [10]. Total organic carbon (TOC) is complementary to chemical oxygen demand (COD) and biochemical oxygen demand (BOD), it is considered a better indicator of organic content as it measures directly the key elements in water theoretically irrespective of the structure of the organic compounds [11]. The treatment of produced water has attracted research attention due to its environmental concerns and the prospect of beneficial uses [12]. Hence, an effective and economically viable method of its treatment is imperative to curtail possible adverse effects on the people and the ecosystem of the oil-bearing communities and to make it suitable for beneficial use.

Different technologies have been employed to treat produced water by different practitioners, but the constituents removed by each technology and the extent of organic compounds removal has to be considered to identify the potential and effective treatment technologies for offshore industrial applications [13]. Different treatment techniques for produced water treatment include adsorption, membrane separation, biological treatment and chemical treatment and recovery among others [14]. Adsorption has been identified as one of the effective methods, widely used in water and wastewater systems among many chemical and physical methods due to its flexibility of design and operation, none generation of toxic substance and ease of recovery of adsorbent after the application [15, 16]. Adsorption is applied for source reduction, wastewater treatment and reclamation for beneficial uses [17].

Activated carbon has been recognized as an effective adsorbent due to the simplicity of design, ability to adsorb numbers of pollutants and fast adsorption kinetics [18]. The high adsorption capacity of activated carbon has been attributed to its high surface area, well developed porous structure and presence of many different types of functional groups [19]. Nevertheless, the application of activated carbon as an adsorbent is limited by its high production and regeneration cost [20]. The application of nanostructured carbon materials as adsorbents has gained global attention on a commercial scale with a special interest in carbon nanotubes (CNTs) due to their specific properties which can be utilized for specific functions, besides, their surface properties can be modified via purification and functionalization to tailor their surface affinity to multiple pollutants [21, 22]. CNTs have been recognized for their excellent removal of pollutants from aqueous solution and have shown good adsorption properties towards organic pollutants [23]. The large adsorption capacity of CNTs has been mainly attributable to their pore structure, surface area and the existence of a wide spectrum of surface functional groups [24]. CNTs surface area is approximately as large as that of activated carbon, their advantage lies in the fact that they have a better arrangement of carbon atom [25]. In addition, the superior adsorption capacity of CNTs compared to activated carbon is credited to the presence of aggregated pores with large mesopores volume and the presence of less negative surface charge [26].

MWCNTs are better candidates due to their special physical and chemical properties and are considered biocompatible in many environmental applications [27]. However, CNTs' efficiency in the environmental application is limited by their surface hydrophobicity. Hence, CNTs are functionalized with other reactive material having appropriate functional groups to improve their efficiency [28]. Functionalization of CNTs using bi-functional molecule such as PSE is pursued to enhance their solubility. While success has been recorded in the biological application of PSE functionalized CNTs [29, 30], there is a paucity of information on their potential application in wastewater treatment. In addition, reports [31, 32] have it that TOC as a non-specific measure is used to measure organic micro-pollutants in wastewater because monitoring of individual pollutants is complicated and expensive. However, scanty information is available on the application of PSE functionalized CNTs for the removal of TOC from produced water. To the best of the authors' knowledge, no study has reported optimum removal efficiency of TOC from produced water using FMWCNTs nano-adsorbent.

In this present study, nano-adsorbent developed from MWCNTs was purified and then Functionalized using PSE to enhanced their adsorption capability for efficient removal of TOC from oil-produced water. The effects of the process parameters; contact time, adsorbent dosage and solution temperature were investigated on the adsorption capacity and CCD of RSM was used to optimize these adsorption process parameters to achieve high adsorption capacity.

2. Materials and methods

2.1. Materials

The kaolin ($Al_2Si_2O_5(OH)_4$) used in this study was obtained from Ejigbo Local Government Area, Lagos State. All the reagents were of analytical grade. Cobalt nitrate hexahydrate ($Co(NO_3)_2.6H_2O$, 98.5 %), nickel nitrate hexahydrate ($Ni(NO_3)_2.6H_2O$, 99.99), iron nitrate nonahydrate ($Fe(NO_3)_3.9H_2O$, 98%) concentrated sulfuric acid (H_2SO_4, 98%), concentrated nitric acid (HNO_3, 99.99%) and 1-pyrenebutanoic acid N-hydroxyl succinimidyl ester ($C_{24}H_{19}NO_4$) (95%) were supplied by Sigma Aldrich. The oil-produced water sample was collected from an oil exploration company in the Niger Delta Area of Nigeria. The water sample was collected in a sealed sterile plastic container and then placed in a refrigerator at 4 °C.

2.2. Preparation of FMWCNTs nano-adsorbent

MWCNTs were synthesized by the catalytic chemical vapor decomposition method [33]. Tri-metallic Fe–Co–Ni/kaolin catalyst was prepared by dissolving 2.33g, of $Co(NO_3)_2.6H_2O$, 2.33g of $Ni(NO_3)_2.6H_2O$ and 3.23g of $Fe(NO_3)_3.9H_2O$ in 40 cm^3 of distilled water. This was followed by the addition of 8.0 g of kaolin ($Al_2Si_2O_5(OH)_4$) support to the solution. The mixture was allowed to age for 30 min at 200 revolutions per minute (rpm) stirring speed. The resulting slurry was then dried in an oven at 120 °C for 12 h, ground into a fine powder, and sieved through a 150 μm sieve screen. The obtained fine powder was then calcined at 400 °C and duration of 16 h. The prepared catalyst was loaded into a quartz boat and placed in the center of the quartz tube. The furnace was heated at 10 °C/min while the carrier gas (Argon) was left to flow over the catalyst at 30 mL/min to eliminate entrapped air from the system. At the pre-set temperature of 700 °C, acetylene was introduced at a flow rate of 100 mL/min and the argon flow rate was increased to 200 mL/min and left to react for 30 min. When the reaction time was attained, the flow of acetylene was stopped while the flow rate of argon was reduced to 30 mL/min and left to flow until the furnace cooled down to room temperature. The boat was removed from the reactor and weighed to quantify the amount of MWCNTs that has been produced. The black powder was collected and stored in an airtight container at ambient temperature.

2.3. Purification and functionalization of CNTs produced

First, 100 mg of synthesized MWCNTs were added to a mixture of concentrated (HNO_3) and (H_2SO_4) in ratio 1:3 (v/v) and sonicated at 45 °C for 3 h to remove the residual metal and other impurities adsorbed in the CNTs [34]. After cooling to room temperature, the mixture was diluted with distilled water and filtered until a pH of 7 was attained. The PMWCNTs sample obtained was oven-dried at 100 °C for 10 h [34]. Then, 3 mg of PMWCNT sample obtained was dispersed in a known volume of 5 mM PSE in methanol and incubated at room temperature for 1 h [30]. The sample was then rinsed 3 to 4 times in methanol to rinse off excess reagent and then oven-dried at 100 °C for 10 h. The resultant FMWCNT powder was kept in an airtight sample bottle and stored at room temperature.

2.4. Characterization of MWCNTs nano-adsorbent

The developed nano-adsorbents were examined by scanning electron microscopy (HRSEM), high resolution transmission electron microscopy (HRTEM), Fourier Infrared Spectroscopy (FTIR) and Brunauer-Emmert-Teller (BET). The morphology of the samples was determined using Zeiss Auriga HRSEM. A small quantity of the sample was spread on a sample holder and sputter coated with Au–Pd using Quorum T15OT for 5 min before analysis. The sputter-coated samples were firmly attached to the carbon adhesive tape and analyzed using Zeiss Auriga HRSEM equipped with In-lens standard detector at 30 kV. The microscope was operated with electron high tension (EHT) of 5 kV for imaging and the detailed structure and morphology of the samples was determined by Zeiss Auriga HRTEM operated at 3950 V. Small quantity of the samples was suspended in 10 ml methanol and ultra-sonicated until it was well dispersed in the solvent. Few drops of the suspension were spread on a carbon grid with lacy carbon thin film and allowed to dry before being transferred to the HRTEM sample chamber for the analysis. A clear picture of the sample was obtained by varying the magnification using a magnification lens. The functional groups were identified using the PerkinElmer FTIR spectrometer. Prior to the sample analysis, the background spectrum of air at ambient condition was running, the spectra of the sample were recorded in the range of 4000 to 500 cm^{-1} with a resolution of $1cm^{-1}$. The specific surface areas and porosity were measured by nitrogen adsorption/desorption at 77 K using Nova 4200e-series equipment.

2.5. TOC analysis

TOC was determined using the method described by Mane *et al* [35], by adding 10 mL of 1 N potassium dichromate and 2 mL of concentrated sulphuric acid to 250 mL conical flask containing 50 ml of sample and left to stand for 30 min. The volume was then adjusted with 150 mL distilled water, 10 mL of orthophosphoric acid and 1 mL Diphenylamine indicator was added to the content of the conical flask and this was titrated with 0.05 N ferrous ammonium sulphate (FAS) till color changes from blue-violet to green. The concentration of TOC in the water sample was then determined using the relationship presented in Eq. (4)

$$TOC = \frac{10(V_b - V_f) \times 0.003}{V_b \times V} \tag{1}$$

Where V_b is the volume of FAS in a blank, V_f is the volume of FAS in the sample and V is the volume of the sample.

The COD was also determined using the method described by Mane *et al* [35], by adding 10 mL of 0.25 N potassium dichromate ($K_2Cr_2O_7$) and 30 mL of sulphuric acid and Silva-sulphate (H_2SO_4+Ag_2SO_4) to COD Vail containing 20 mL of the sample. The solution was digested for 2 h in the COD digester. The sample was then brought out and allowed to cool to ambient temperature. The solution was then diluted to 150 mL with distilled water and the excess $K_2Cr_2O_7$ remained was titrated with ferrous ammonium sulphate (FAS) using ferroin indicator. The concentration of COD in the water sample determined from the relationship presented in Eq. (2)

$$COD = \frac{(a-b) \times N \times 1000 \times 8}{V} \tag{2}$$

Where a is the mL of FAS used for the blank, b is the mL of FAS used for the sample, N is the normality of FAS and 8 is the milliequivalents of oxygen, and V is the volume of the sample.

2.6. Batch adsorption studies

The batch adsorption experiments were carried out at 30 ° C by adding 0.02, 0.04, 0.06, 0.08 and 0.1 g of FMWCNTs adsorbent in a 250 ml conical flask, each containing 100 mL produced water. The flasks were sealed and placed in a thermostated shaker operated at 150 rpm and allowed to attain equilibrium. The kinetics of adsorption experiments were conducted at a different time interval (10, 20, 30, 40, 50, and 60 min). The effect of temperature was investigated at different temperatures (30, 40, and 50 °C). After each experiment, the flasks were brought out of the shaker and the sample was filtered through a 0.45-μm membrane filter to separate the spent adsorbent. The final concentration of TOC in produced water was determined using the method described by Mane *et al.* [35]. The uptake efficiency of the nano-adsorbent was calculated using Eq. (3)

$$\text{Percentage TOC uptake} = \frac{Co - Ce}{Co} X100 \tag{3}$$

Where C_o is the initial concentration of pollutants in mg/L and C_e is the final concentration of TOC at equilibrium.

The amount of pollutants adsorbed at equilibrium was calculated using Eq. (4)

$$q_e = \left(\frac{C_o - C_e}{m}\right) V \tag{4}$$

Where; q_e, is the amount of TOC adsorbed at equilibrium (mg/g), C_o is the initial concentration of TOC molecule (mg/L), C_e is the equilibrium pollutants concentration in solution (mg/L), m is the mass of adsorbent (g)

2.7. Experimental design for TOC removal from produced water

The central composite face-centered design was employed to capture the effects of three essential adsorption process variables: (I) contact time, (J) solution temperature, and (K) adsorbent dosage on the responses (removal of TOC). The numerical factors were varied over 3-level plus and minus one axial point, plus and minus one (1) factorial point and one center point. The variables, the coded and actual values are as presented in Table 1. The experimental results of the response surface methodology were fitted using second order polynomial Eq. (5)

$$Y = \alpha_o + \sum \alpha_{ii} B_i + \left(\sum \alpha_{ii} B_i\right)^2 + \sum \alpha_{ij} B_i B_j \tag{5}$$

Where Y is the predicted responses (TOC removal), α_o is the constant, $\alpha_{ii}$is the quadratic coefficients. α_{ij}, is the interaction coefficients, and B_iB_j are the coded values of the chosen variables. Analysis of variance (ANOVA) was carried out to establish the significance of the quadratic model at a 95 % confidence interval and Design Expert Version 6.0.8 (Stat Ease, Inc., Minneapolis, MN 55413, USA) was used for the quadratic model fitting.

2.8. Adsorption kinetics study

The adsorption mechanism of TOC on FMWCNTs was investigated using pseudo-first-order, pseudo-second-order, Elovic, and intra-particle diffusion models.

2.8.1. Pseudo–first–order kinetic equation

The Lagergren' [36] pseudo-first-order Equation is generally expressed as:

$$\frac{dq_t}{d_t} = k_1(q_e - q_t) \tag{6}$$

Where q_e and q_t are the sorption capacity (mg/g) of the FMWCNTs nano-adsorbent at equilibrium and any time t respectively, and k_1 (min^{-1}) is the rate constant of pseudo-first order adsorption. Integrating Eq. (6) and applying the boundary condition $q_t = 0$ at t = 0 and q_t at t = t, Eq. (6) becomes linear as presented in Eq. (7)

Table 1. Variation of variables at the center point.

Variables	Unit	Symbols	Coded values	Actual values	
			-1	0	+
Contact time	(min)	I	10	30	50
Solution temperature	(°C)	J	30	40	50
Adsorbent dosage	(g)	K	0.02	0.06	0.1

$$Log(q_e - q_t) = Logq_e - \frac{k_1 t}{2.303} \quad (7)$$

Pseudo-first-order rate constant and equilibrium adsorption capacity are estimated from the slope and intercept of linear plot of $Log(q_e - q_t)$ versus t, respectively.

2.8.2. Pseudo-second-order kinetic model

Pseudo-second-order kinetics model [37] is given as Eq. (8)

$$\frac{dq_t}{d_t} = k_2(q_e - q_t)^2 \quad (8)$$

Integrating Eq. (8), the linear form, Eq. (9) is obtained

$$\frac{t}{q_t} = \frac{1}{k_2 q_e{}^2} + \frac{t}{q_e} \quad (9)$$

Where k_2 ($gmg^{-1}min^{-1}$) is the Pseudo second-order equilibrium rate constant. The plot of $\frac{t}{q_t}$ versus t gives a linear relationship and then k_2 and q_e can be determined from the slope and intercept of the line, respectively. The initial rate of adsorption h ($mgg^{-1}min^{-1}$) when $t \rightarrow 0$, could be obtained from Eq. (10)

$$h = k_2 q_e{}^2 \quad (10)$$

2.8.3. Elovic kinetic model

The Elovic model is given as

$$q_t = \frac{1}{\beta_d} ln(\alpha_a \beta_d) + \frac{1}{\beta_d} ln(t) \quad (11)$$

Where α_a ($mgg^{-1}min^{-1}$) is the initial rate of adsorption and β_d (g/mg) is the desorption constant related to extent of the surface coverage and activation energy for chemisorption.

The kinetics constants α and β are determined from the slope and intercept of the plot of $q_t$versus $\ln t$, respectively.

2.8.4. Intra-particle diffusion model

To investigate the diffusion mechanism, intra-particle diffusion mode expressed as Eq. (12) was used

$$q_t = K_p t^{1/2} + C \quad (12)$$

Where K_p is the intra-particle diffusion rate constant ($mgg^{-1}min^{-1/2}$) and C (mg/g) is the intercept whose value gives information about the boundary layer thickness. The value of K_p and C are calculated from the slope and intercept of the linear plot of q_t versus $t^{1/2}$, respectively.

2.9. Adsorption isotherms study

The equilibrium data were analyzed using Langmuir, Freundlich and Harkins-Jura isotherms model to describe the relationship between the adsorbent and the adsorbed TOC.

2.9.1. Langmuir isotherm model

The Langmuir isotherm model expressed as Eq. (13) was employed to determine the maximum adsorption capacity obtained from complete monolayer coverage of TOC on the surface of the nano-adsorbent.

$$q_e = \frac{q_o \alpha_L C_e}{1 + \alpha_L C_e} \quad (13)$$

The linear form of Eq. (13) is expressed as Eq. (14)

$$\frac{1}{q_e} = \frac{1}{q_o} + \frac{1}{\alpha_L q_o C_e} \quad (14)$$

Where q_e (mgg^{-1}) is the adsorption capacity of TOC by the adsorbent at equilibrium, q_o (mgg^{-1}) is the maximum monolayer TOC adsorption capacity, α_L (Lmg^{-1}) is the Langmuir isotherm constant related to the free energy of adsorption and C_e (mgL^{-1}) is the equilibrium concentration of TOC in solution. Langmuir isotherm fit the sorption process if a plot of $\frac{1}{q_e}$ versus $\frac{1}{C_e}$ gives a straight line. $\frac{1}{\alpha_L}$, and $\frac{1}{q_o}$ are obtained from the slope and intercept of a linear plot, respectively.

The dimensionless equilibrium parameter is known as the separation factor (R_L) used to analyze Langmuir isotherm is expressed as Eq. (15)

$$R_L = \frac{1}{1 + \propto_L C_o} \quad (15)$$

The value of R_L gives information about the favorability of the isotherm, the adsorption is favorable if R_L value lies between 0 and 1, unfavorable ($R_L > 1$), linear ($R_L = 1$), or irreversible ($R_L = 0$).

2.9.2. Freundlich isotherm

The Freundlich isotherm is expressed as Eq. (16)

$$q_e = K_f C_e{}^n \quad (16)$$

The linear form of Eq. (16) is expressed in logarithm form given in Eq. (17)

$$Logq_e = LogK_f + nLogC_e \quad (17)$$

Where q_e (mgg^{-1}) is the amount of TOC adsorbed at equilibrium, K_f is Freundlich constant related to adsorption capacity and n is the heterogeneity coefficient. These two parameters are obtained from the plot of Log q_e versus, Log C_e.

2.9.3. Harkin-Jura isotherm

Harkin-Jura adsorption isotherm can be expressed as Eq. (18)

$$q_e = \left(\frac{A_H}{B_H - LogC_e}\right)^{1/2} \quad (18)$$

And the linear form is expressed as given in Eq. (19)

$$\frac{1}{q_e{}^2} = \left(\frac{B_H}{A_H}\right) - \left(\frac{1}{A_H}\right) LogC_e \quad (19)$$

Where the Harkin-Jura isotherm constants A_H and B_H are obtainable from the plot of $\frac{1}{q_e{}^2}$ versus. $LogC_e$

3. Results and discussion

3.1. Characterization of carbon nano-adsorbent

This study focused on the development of nano-adsorbent from CNTs for the removal of TOC from oil-produced water. HRSEM was used to

study the morphology, alignment, the density of the tubes and the purity of the grown tube bundle. The HRSEM micrographs of as-produced, purified and functionalized MWCNTs are shown in Figure 1a, b, and c, respectively. The HRSEM image in Figure 1a revealed compactly interwoven like structured MWCNTs of non-uniform diameters with several micrometers in length. It was noted that the grown MWCNTs have non-homogeneous wall structure morphology as some are hollow while some are spiral (red arrow) as revealed in the HRSEM micrograph. It can also be seen that the as-produced MWCNTs contain some impurities such as amorphous carbon, support and catalyst nanoparticles. The black spots indicated by the yellow arrow in the HRSEM image represent the catalyst while the presence of the support or/and carbonaceous impurities is denoted by a dotted circle.

Metal impurities are normally found in as-synthesized MWCNTs from the CVD process due to residue from the transition metal catalyst [38]. After refluxing in a mixture of nitric and sulphuric acid, there was a remarkable reduction in the metal impurities, while the presence of support or/and amorphous can still be seen as shown by the yellows circle in Figure 1b. The presence of amorphous carbon in CNTs could particularly enhance the adsorption capacity of organic chemicals onto the surface of CNTs [39]. It is worthy of note that the purification process generates various functional groups, cut and shorten CNTs [40] after the purification, the MWCNTs became more homogenous and some of the tangled and bent MWCNT become straightened as indicated by the blue arrow in Figure 1b, indicating less structural defect. Tangling is an indication of large structural defects in CNTs [41]. In addition, the purified MWCNTs appeared less compacted compared to the as-produced CNTs. This may be attributed to the presence of functional groups introduced by the acid purification and these functional groups are believed to cause a reduction in the force of attraction which facilitates dis-bundling of the CNTs into the individual tube, enhanced it solubility in most organic solvents thereby give room for further modifications of CNTs such as functionalization [42].

The HRSEM image of FMWCNTs (Figure 1c) revealed a shining spongy like morphology confirming that the PSE molecule was successfully incorporated on the outer wall of the MWCNTs (arrow). Moreover, the rough surface morphology of FMWCNTs observed may be linked to the agglomeration of the MWCNTs tubes resulted from the functionalization process and this suggested that the FMWCNTs would aggregate pollutants. In addition, the MWCNTs appeared less-tangled after the functionalization process and suggested an enhanced adsorption capability of the FMWCNTs. The amine group present in PSE may facilitate electrostatic attraction with the negative charges on the organic compound in oil-produced water, hence improves the wettability and consequently the adsorption capability. The morphology of MWCNTs adsorbents was also obtained after the application for TOC removal from oil-produced water and the result of HRSEM is presented in Figure 1d. It was observed that the surface of the spent adsorbent was coated by the recovered pollutants. This may be an evidence of efficient adsorption of TOC onto the surface of the outer-wall of clustered MWCNTs structures. It was noted that the MWCNTs' structure was retained after the application, though trivial MWCNTs cut and shortening were observed.

The HRTEM image Figure 2 corroborates the HRSEM results. The HRTEM in Figure 2a revealed the presence of impurities such as catalyst nanoparticle support and amorphous carbon as indicated by arrows. Figure 2b confirmed the effectiveness of the purification method adopted as fewer impurities were left after the purification as confirmed by the EDX (Fig 3a and b, XRD (Figure 4), and Raman (Figure 5), and also showed that the MWCNTs were produced via tip grow (arrow). HRTEM image of FMWCNTs presented in Figure 2c confirmed the attachment of

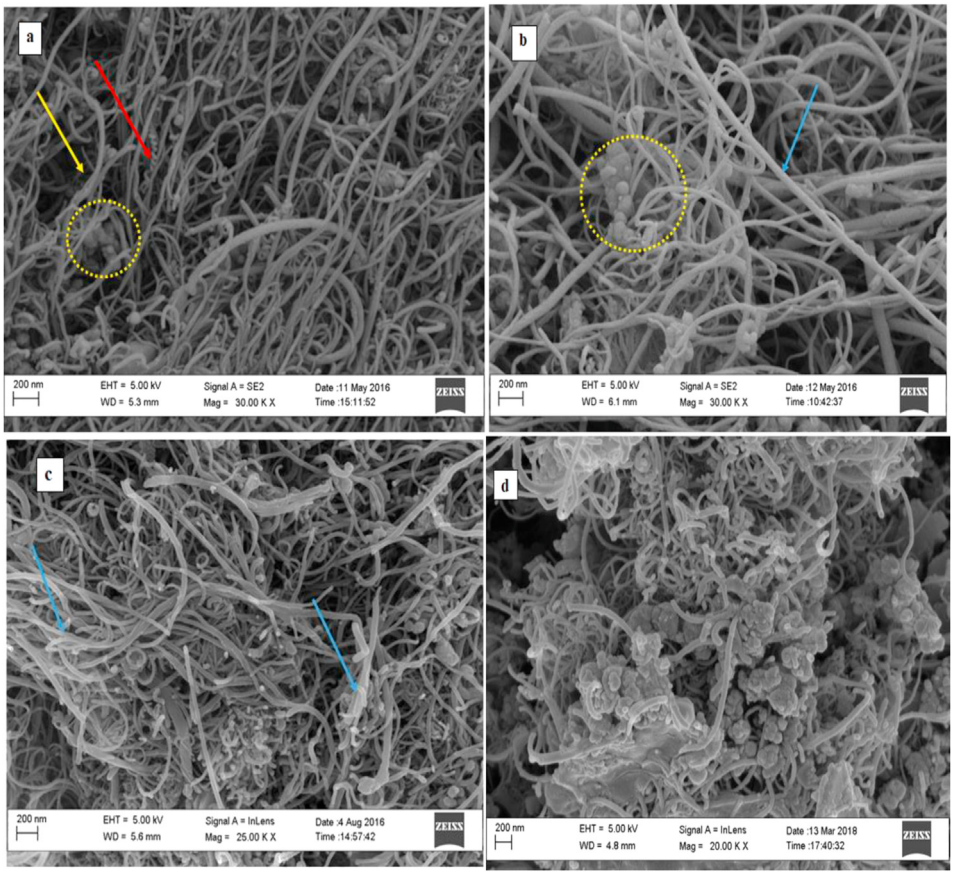

Figure 1. HRSEM of the Developed nano-adsorbent (a) as-produced MWCNTs, (b) PMWCNTs (c) FMWCNTs and (d) Spent adsorbent.

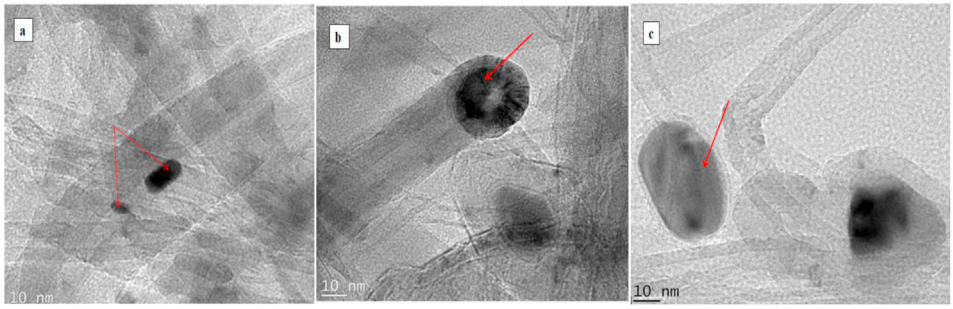

Figure 2. HRTEM of the Developed nano-adsorbent (a) as-produced MWCNTs, (b) PMWCNTs (c) FMWCNTs.

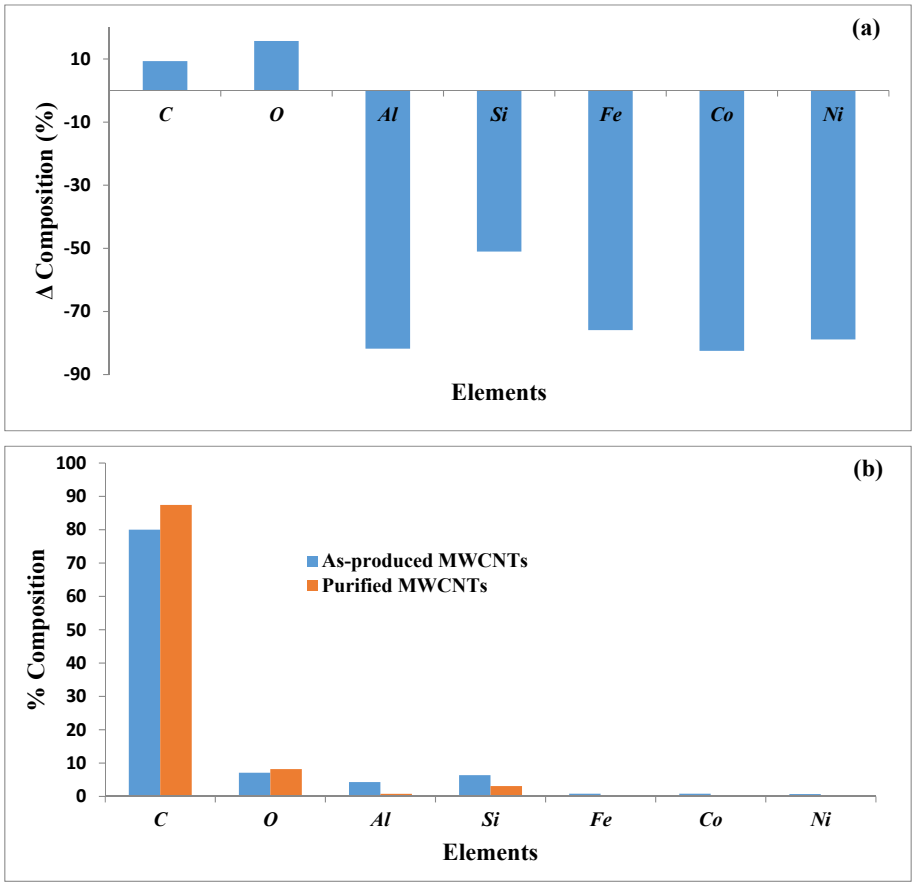

Figure 3. (a) Change in percentage composition of elements in the as-produced MWCNTs after purification. Result based on EDX elemental analysis of as-produced and purified MWCNTs in (b).

the PSE molecule on the surface of the MWCNTs. This is evident by the observation of a thick black egg-shaped cluster attached to the surface of the FMWCNTs.

Further, the X-ray diffraction patterns of unpurified and purified MWCNTs presented in Figure 4 showed that the purity of carbon in MWCNTs was significantly enhanced by the purification process. The intensity of peaks due to graphitized carbon of CNTs around 2θ of 26° (002) and 44° (100) planes was higher in the purified sample than the as-produced sample. Especially, the peak at 2θ of 35.51° which may be due to impurities found in unpurified CNTs disappeared after purification. Raman spectroscopy analysis of the as-produced and purified carbon nanotubes shown in Figure 5(a) and (b) indicated that the weak and broad peaks in the as-produced sample were narrowed to form sharp peaks after purification. In both samples, radial breathing modes (RBMs) were observed in the low frequency region (100–200 cm^{-1}), and these are associated with large diameter tubes of the MWCNTs under study [43]. The most important features seen in Figure 5(a) are the disorder induced *D* band at 1320–1370 cm^{-1}, and the tangential *G* band at 1530–1610 cm^{-1} which are related to the graphite tangential E_{2g} Raman active mode where the two atoms in graphene unit cell are vibrating tangentially one against the other [43]. The *D* mode indicates the disordered features of the carbon and defects in the curved graphite sheet, sp^3 carbon with other impurities while the *G* mode is associated with the ordered crystalline graphite in the CNTs [44]. The Raman spectrum shows a second-order harmonic band *G*' (Graphite) at 2426 cm^{-1} and 2664 cm^{-1}, and a peak at 3638 cm^{-1} corresponding to the *D* + *G* band.

Depicted in Figure 6 is FTIR spectra of as-produced MWCNTs, PMWCNTs, and FMWCNTs. The FTIR spectra of as-produced MWCNTs showed fewer weak absorption peaks at 2973 cm^{-1} corresponding to C–H stretch; 1534 cm^{-1}, for MWCNTs C=C stretch and 1023 cm^{-1}C–O stretching vibration [45,46]. The formation of new absorption bands was

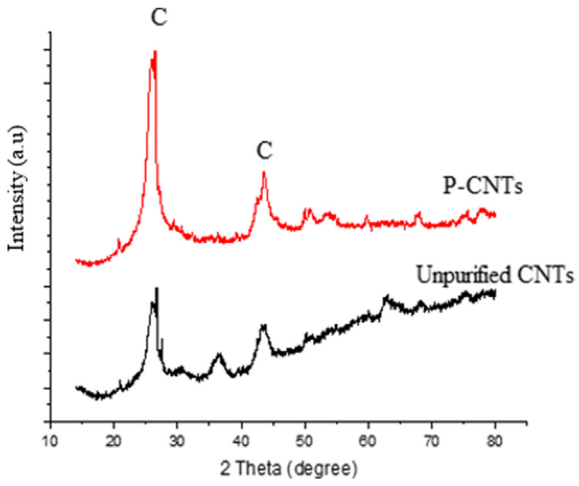

Figure 4. XRD spectra of (a) as-produced and (b) PMWCNTs.

obvious after the purification of the MWCNTs. Additional peaks were observed at1630, 2630 and 3250 cm^{-1}corresponding to C=O stretch C-H_x stretch and–OH stretch, respectively. The shift in the w C=C stretch to a higher wavenumber may be an indication of the change in the MWCNTs structure upon acid purification as Infrared (IR) wavenumber (1600cm^{-1}) depend on the geometry and the diameter of the tube [46, 47]. The incorporation of PSE on the surface of MWCNTs resulted in the appearance of additional peaks at 1156 and 2346 cm^{-1}corresponding to N–C stretching vibration attributed to the incorporation of amine group [48] and C–O stretching vibration for ester [27]. The additional functional groups formed on the surface of FMWCNTs due to the incorporation of PSE provided new adsorption site for the removal of TOC from oil-produced water.

The surface area of adsorbent is also very vital to the adsorption process as porous material with a high surface area may be employed as adsorbent [49]. The high adsorption capacity of CNTs is attributed to their large surface area [50]. The BET analysis revealed that the surface area of as-produced MWCNTs, PMWCNTs and FMWCNTs is 970.17 m^2/g, 869.25 m^2/g and 831.80 m^2/g, respectively. This result is consistent with the surface area reported [27, 51] for similar materials. The reduction noticed in the surface areas of purified and functionalized MWCNTs may be attributed to the presence of functional moieties on the internal and external of the surface of the MWCNTs as a result of the acid oxidation and polymer agglomeration [15, 52] as confirmed by the FT-IR (Figure 6) and HRSEM image. The existence of these functional groups provided the various binding site for pollutants fixation.

3.2. Batch adsorption study

The batch adsorption studies have been extensively reported in the literature [15, 49] as a simple and reproducible methodology usually performed to provide vital information on the behavior of the adsorbent. The developed nano-adsorbents (PMWCNTs and FMWCNTs) were employed for adsorption of TOC from Produced water by batch adsorption studies. The performance efficiency of the PMWCNTs and FMWCNTs nano-adsorbent was examined with TOC initial concentration of 55.53 mg/g under the same batch adsorption condition: 0.02 g adsorbent dosage, 10–90 min contact time and 30 °C solution temperature. Figure 7 showed that the removal efficiencies of PMWCNTs and FMWCNTs increased as the contact time increased until the equilibrium time was reached beyond which no more TOC is removed. It was noticeable from Figure 7 that the FMWCNTs did not only exhibit a fast adsorption rate but also showed superior performance efficiency compared with PMWCNTs. The FMWCNTs achieved about 93.6% removal efficiency within 30 min of the adsorption process, while the removal efficiency of PMWCNTs increased gradually from 72% to about 78.3% within 70 min of the adsorption process. High adsorption rate, high selectivity and fast kinetics are vital to the selection of the most promising adsorbent [49] FMWCNTs. The fast adsorption rate of FMWCNTs may be attributed to the possibility of pyrene in PSE to form π-π interaction with CNTs leading to sidewall non-covalent functionalization of CNTs; consequently, this facilitates the solubility of CNTs in water, increased the adsorption energy and thus improved the removal capability of FMWCNTs [53, 54]. In addition, it is obvious from the FTIR result shown in Figure 6 that the incorporation of PSE in FMWCNTs resulted in the formation of additional functional groups, which created more chemical adsorption sites on the surface of FMWCNTs and thereby enhanced the dispersion of FMWCNTs in the liquid phase and made them more suitable for the adsorption of TOC. FMWCNTs were chosen as the preferred adsorbent for the adsorption process because it posits a more viable route for industrial application.

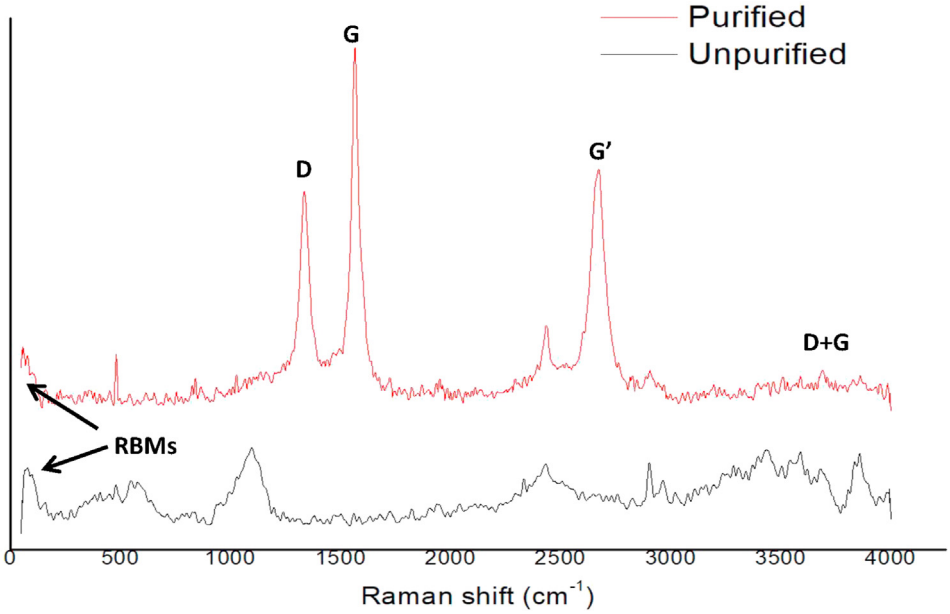

Figure 5. Raman Spectra of as-produced, and PMWCNTs.

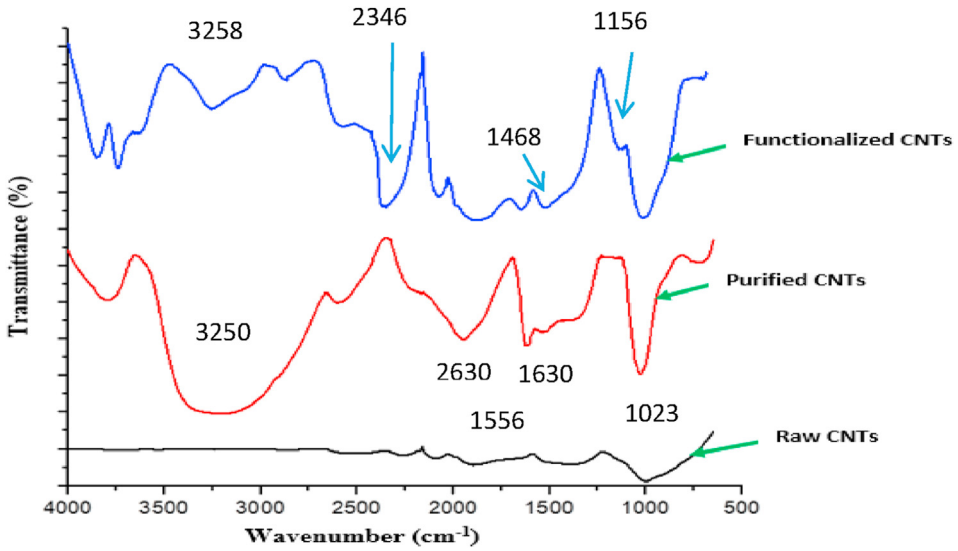

Figure 6. FTIR Spectra of as-produced MWCNTs, PMWCNTs and FMWCNTs.

3.2.1. *Effect of contact time, solution temperature and adsorbent dosage on TOC uptake from produced water*

Several studies [15, 51, 55], have demonstrated the importance of adsorption process parameters: contact time, solution temperature and adsorbent dosage to batch adsorption process. The influence of contact time from 10-60 min was investigated on the adsorption capacity of TOC in the temperature range of 303–323K and adsorbent dosage of 0.02–0.1g. The results depicted in Figure 8 indicated that the sorption process occurs at a faster rate and the adsorption capacity increased with the contact time, then, followed by a slower adsorption rate until equilibrium time was reached when no remarkable TOC removal was observed. The fast adsorption rate at the initial period was due to a high driving force in the solid/liquid phase, leading to the fast removal of the TOC by the FMWCNTs adsorbent [51]. The slow adsorption rate noted with time as the reaction progressed may be attributed to the saturation of the external surface of the FMWCNTs nano-adsorbent by the TOC which resulted in diffusion of the TOC into the pore and binded by the internal surface of the nano-adsorbent [56].

It was found that equilibrium was attained in about 40 min corresponding to 259.7 mg/g at adsorbent dosage of 0.02 g and temperature of 303K. Similar trend was noticed for all the adsorbent doses as shown on Figure 8. Nevertheless, a decrease in adsorption capacity with increased in adsorbent doses was noted. The increase in the adsorption rate with increasing adsorbent dosage is linked to increase in surface area and available sorption site for binding TOC on the FMWCNTs nano-adsorbent surface resulted from increased in dosage while the decreased in adsorption capacity with increased in adsorbent dosage may be ascribed to the saturation of the adsorption site by TOC [57]. The high adsorption capacity of FMWCNTs may be attributed to high surface area, availability of more surface functional groups, nature of the adsorbent and the adsorbate.

In addition, Figure 8 showed that the sorption capacity of FMWCNTs decreased as the temperature increased from 30-50 °C (303–323K) for all the adsorbent doses considered in this study, implying that the adsorption of TOC to FMWCNTs was exothermic and the FMWCNTs nano-adsorbent affinity for TOC was higher at lower temperature. The decreased in adsorption capacity with increasing solution temperature may be ascribed to the high kinetic energy of TOC which prevented them from binding to the active site on the surface of FMWCNTs nano-adsorbent and reduction in the boundary layer of the nano-adsorbent owing to higher tendency of TOC to desorb from the pores [23]. Hence the kinetics study at various doses was carried out at 30 °C.

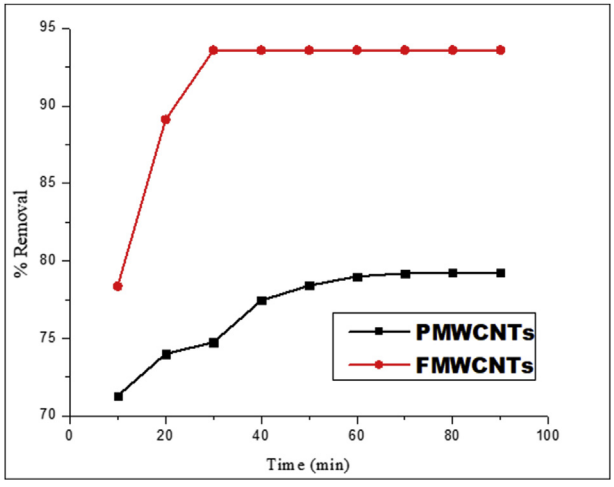

Figure 7. Performance evaluation of PMWCNTs and FMWCNTs at contact time (30 min), adsorbent dosage 0.02 g, solution Temperature (303K).

3.3. *Modeling of TOC removal by RSM*

Central composite design of response surface methodology was applied to optimize three individual adsorption process parameters related to water treatment in order to facilitate cost-effective adsorption process. The response (adsorption capacities) was ranged from 55.33 to 259.85 mg/g as depicted in Table 2. Quadratic polynomial regression model of CCD was used to analyze the experimental data. All the main effects and their interactions were calculated; the regression coefficients were obtained. In the model Equation, the terms found to be insignificant were ignored and the final Equation in terms of coded factors, Eq. (20) follows;

$$\text{Adsorption capacity for TOC sorption}(q_e) = 86.56 + 12.67\text{I} - 5.21\text{J} - 87.64\text{K} + 64.20\text{K}^2 - 13.95\text{IK} + 6.12\text{JK} \quad (20)$$

Based on the quadratic polynomial Eq. (20), it was found that the contact time has synergetic single effects on adsorption capacity while the solution temperature and the adsorbent dosage have antagonistic effects on the adsorption capacity. This predicted trend was consistent with the experimental results which showed that the adsorption capacity decreased with increasing solution temperature and the adsorbent

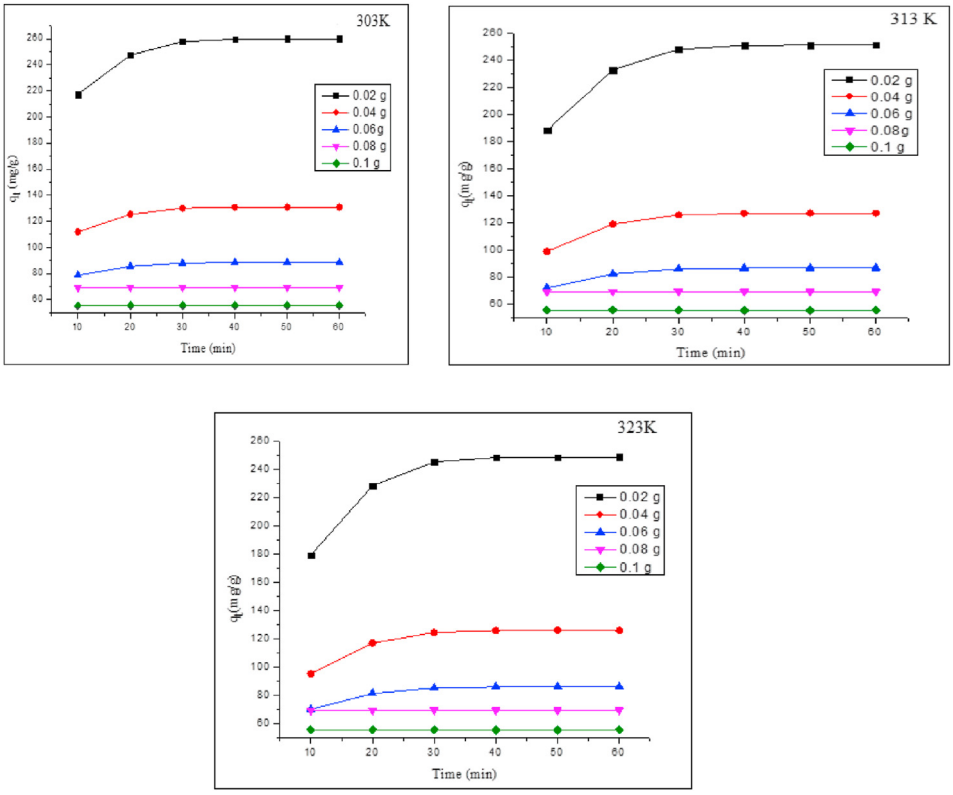

Figure 8. Effect of time and adsorbent dosage on removal of TOC at temperatures (303, 313 and 323K).

dosage as presented in section 3.2.1. Only adsorbent dosage had significant quadratic effect on the adsorption capacity. The interaction of contact time and adsorbent dosage had negative effect on the adsorption capacity for TOC removal while the interaction between adsorbent dose and solution temperature has positive effects on the adsorption process but the interaction of contact time and solution temperature did not have any significant effect [58].

The adequacy and significance of the developed quadratic polynomial model for the sorption process were evaluated using the Fisher F-test and p-value of the analysis of variance ANOVA presented in Table 3. The goodness of fit was accessed by coefficient of determination R^2 which showed the variability in response predicted by the independent variables [59]. The R^2, adjusted R^2 and predicted R^2 were found to be 0.9959, 0.9923, and 0.9547, respectively. With a difference of less than

Table 2. Modeling of TOC removal by RSM.

S/N	Coded value			Contact time (min)	Actual value		Response
	I	J	K		Solution temperature (°C)	Adsorbent dose (g)	TOC (mg/g)
1	1	1	-1	50.00	50.00	0.02	248.67
2	0	0	0	30.00	40.00	0.06	85.78
3	0	0	1	30.00	40.00	0.10	55.47
4	0	0	0	30.00	40.00	0.06	85.78
5	0	0	0	30.00	40.00	0.06	85.78
6	0	1	0	30.00	50.00	0.06	85.11
7	0	0	0	30.00	40.00	0.06	85.78
8	0	0	0	30.00	40.00	0.06	85.78
9	-1	0	0	10.00	40.00	0.06	71.98
10	-1	-1	-1	10.00	30.00	0.02	217.3
11	-1	1	1	10.00	50.00	0.10	55.33
12	1	0	0	50.00	40.00	0.06	86.48
13	1	1	1	50.00	50.00	0.10	55.47
14	0	0	-1	30.00	40.00	0.02	248.27
15	0	0	0	30.00	40.00	0.06	85.78
16	-1	-1	1	10.00	30.00	0.10	55.41
17	0	-1	0	30.00	30.00	0.06	87.98
18	1	-1	-1	50.00	30.00	0.02	259.85
19	-1	1	-1	10.00	50.00	0.02	179.4
20	1	-1	1	50.00	30.00	0.10	55.49

0.2, the predicted R^2 is in reasonable agreement with the adjusted R^2 [60]. The model F-value of 271.45 indicated that the model was significant (P- value <0.0001) and implied that the predicted model adequately represented the data for the adsorption TOC. The adequacy of precision which measures the signal to noise ratio should be more than 4 [58] and in this study was found to be 48.11 indicating adequate signal.

The 3D response surface plots of the interaction effects of three parameters on the adsorption capacity for TOC removal were presented in Figure 9. Figure 9a showed that the effect of contact time and adsorbent dosage on adsorption capacity at constant temperature and Figure 9b depicted the influence of adsorbent dosage and solution temperature at constant contact time on the adsorption capacity. As shown in Figure 9, the interaction of three parameters has different effects on the adsorption capacity for TOC removal from oil-produced water.

Numerical optimization of the model Eq. (20) was carried out using design expert (6.0.8) software package to determine condition that maximize the adsorption capacity for TOC removal from oil-produced water. The goal for the adsorption capacity was set to maximum as required while the contact time, solution temperature, and adsorbent dosage were set to be in range. The optimum condition was selected based on the highest desirability which normally ranged from zero to 1 [61]. The numerical optimization produced an optimum adsorption capacity for TOC of 260 mg/g at contact time of 49.70 min, solution temperature of 34.81 °C and dosage of 0.02 g having desirability of one. The optimal solution confirmed the operating parameters that maximize the adsorption process.

To verify the model prediction, the validation experiment was carried out under the predicted optimal conditions; and the adsorption capacity of 257.8 mg/g was achieved for TOC removal from oil-produced water. The result obtained indicated that the corresponding average TOC removal was within the predicted values of the model. This result corroborated the effectiveness of the RSM for optimum TOC removal from crude oil-produced water.

The raw and treated produced water at the optimum condition were characterized for their physicochemical properties, and the results are presented in Table 4. As shown in Table 4, most of the parameters considered were considerably high and significantly exceeded the acceptable limit. This may be linked to the geological characteristics of the reservoir, the chemical composition of oil and gas phases in the reservoir and the added chemicals [62, 63]. After treating with the FMWCNTs nano-adsorbent, there was appreciable reduction of these contaminants, though the value of conductivity and TDS were still quite high. Conductivity, according to EPA [11] does not have any direct health or sanitary significant, however it is an indication of the present of dissolved ionisable solids. It was observed that the pH, dissolved oxygen (DO) and biological oxygen demand (BOD) of the untreated produced water were found to fall within EPA [11] and NIS [64] standards. This is possibly due to the pre-treatment of the oil-produced water with activated sludge wastewater treatment plant. Interestingly, it was found that the FMWCNTs adsorbent was also effective for the removal of COD and phenol suggesting its potential and capability for removal of organic contaminants.

3.4. Adsorption kinetics study

Adsorption kinetics study is very vital as it provides important information about the reaction pathway and, rate-controlling mechanism [61, 65]. The kinetics of TOC were analyzed by pseudo-first order, pseudo-second order, Elovic models and the adsorption mechanism examined by intra-particle diffusion model. The rate constants were estimated from the linearized plots presented on Fig 10 (supplementary), and were shown in Table 5. The applicability of the kinetics models for the adsorption of TOC was tested by R^2 and Residual Sum of Square Error (RSSE). The results indicated that the R^2 obtained for pseudo-second-order were remarkably high with values > 0.999 for all the adsorbent doses studied. Moreover, the RSSE obtained were also very low, implying that the kinetics of TOC onto FMWCNTs is best described by pseudo-second-order model. The results in Table 5 also revealed that there was a good agreement between the experimental and calculated $q_e$values which also attested to the goodness of fit. The rate constants for pseudo-second order increased from 0.0019 to 1.08 $gmg^{-1}min^{-1}$as the dosage increased from 0.02 to 0.1 g, implying that the adsorption is rapid at the higher dosage and reached equilibrium faster than at the lower dosage [66]. Pseudo-first-order model was poorly correlated with predicted q_e values far less than that obtained from the experiment. Intra-particle diffusion and Elovic models were fairly correlated compared with pseudo-first-order model. The adsorption mechanism showed that the adsorption process is not solely controlled by intra-particle diffusion since the Weber Morris linear plots of $q_t$versus $t^{1/2}$ did not pass through the origin [67]. The adsorption of TOC onto FMWCNTs nano-adsorbent was best described by pseudo-second-order kinetic model which supported the assumption that chemisorption is the rate-limiting. This reaction mechanism suggested ion exchange between TOC and the oxygen containing surface functional group on the FMWCNTs nano-adsorbent [68]. Similar kinetics result was obtained by Sajab *et al* [69] for the removal of TOC from bleaching effluent from pulp and paper mill using chemically treated oil palm empty fruit fiber. Based on the R^2 value and RSSE obtained, the trend is Pseudo second order > Elovic > Intra-particle diffusion > Pseudo first-order kinetic model for TOC removal from produced water.

Table 3. ANOVA for the TOC uptake.

Source	Sum ofSquare	DF	Mean Squares	F Value	Prob > F
Model	97963.36	9	10884.82	271.45	<0.0001*
A	1605.29	1	1605.29	40.03	<0.0001*
B	271.44	1	271.44	6.77	0.0264*
C	76807.70	1	76807.70	1915.47	<0.0001*
A^2	196.36	1	196.36	4.90	0.0513
B^2	3.64	1	3.64	0.091	0.7695
C^2	11334.51	1	11334.51	282.67	<0.0001*
AB	89.78	1	89.78	2.24	0.1654
AC	1556.82	1	1556.82	38.82	<0.0001*
BC	300.13	1	300.13	7.48	0.0210*
Residual	400.99	10	40.10		
Lack of Fit	400.99	5	80.20		0.0623
Pure Error	0.000	5	0.000		
Cor Total	98364.35	19			

*significant at P-value <0.05.

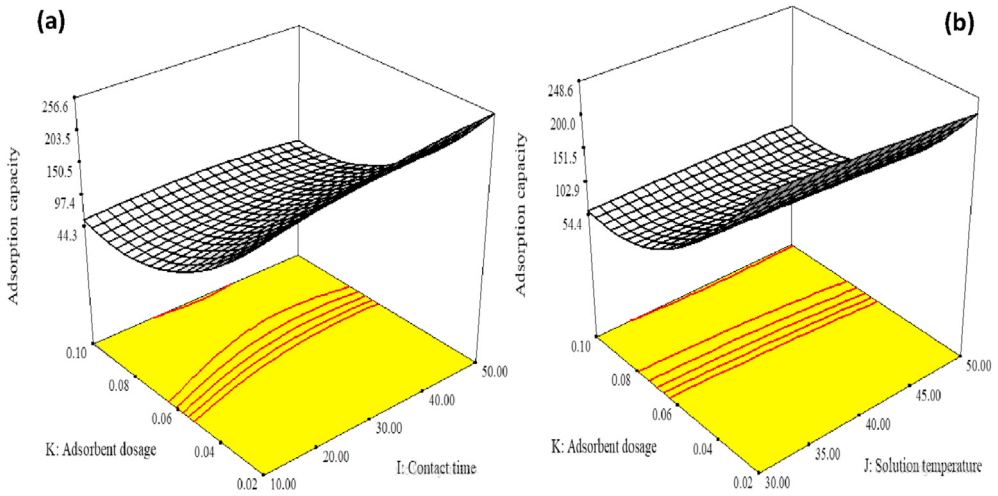

Figure 9. 3D response surface plots: (a) effect of adsorbent dosage and contact time on adsorption capacity, (b) effect of solution temperature and adsorbent dosage.

Table 4. Physicochemical properties of raw and FMWCNTs-treated water at optimum condition.

Physicochemical properties	Raw Produced Water	FMWCNTs-treated Water	EPA/NIS
pH	6.5	7.8	6.5–8.5
Conductivity (μS/cm)	22440	13600	1000
TDS (mg/L)	12100	6700	500
Turbidity (NTU)	11.53	1.9852	5.00
TOC (mg/L)	55.53	0.0249	5.00
DO (mg/L)	4.75	1.45	5–6
BOD (mg/L)	2.8	0.25	6–7
COD	874.67	48.5	40.00
Phenols ($x10^{-3}$ mg/L)	10.9	0.13	1.0
Nitrite (mg/L)	3.16	0.18	0.20
Nitrate (mg/L)	350	120	50

Table 5. Rate parameters for uptake of TOC at various doses of adsorbent and 303 K.

Linear Kinetic model	Dosage				
	0.02 g	0.04g	0.06g	0.08g	0.1g
$q_e$experimental (mg/g)	259.85	130.93	88.45	69.37	55.50
Pseudo-first-order					
k_1 (min^{-1})	-0.0683	-0.1064	-0.0977	-0.1318	-0.1396
q_e (mg/g)	10.8447	10.7453	6.0323	0.4730	0.4455
R^2	-0.0122	0.5242	0.3695	0.9381	0.9430
RSSE	2.7711	2.2947	1.6142	0.4988	0.5126
Pseudo-second-order					
k_2 ($gmg^{-1}min^{-1}$)	0.0036	0.0086	0.0173	1.3011	2.2464
q_e(mg/g)	270.27	132.98.	89.45	69.40	55.49
ho ($mgg^{-1}min^{-1}$)	263.16	152.67	138.70	6265.66.	6918.021
R^2	0.9989	0.9992	0.9995	1	1
RSSE	3.79×10^{-5}	1.12×10^{-4}	1.34×10^{-4}	3.37×10^{-8}	5.24×10^{-8}
Elovic					
α (mgg-1min-1)	97.30	50.16	35.33	31.80	25.44
β (g/mg)	0.0155	0.0309	0.0460	0.0598	0.0748
R^2	0.8972	0.8862	0.8649	0.7835	0.7835
RSSE	4722.08	1331.43	726.74	743.63	475.95
Intra-particle diffusion					
k_{int} (min^{-1})	31.82	15.93	10.63	8.012	6.41
C_{int} (mg/g)	58.82	30.64	21.91	20.23	16.18
R^2	0.73463	0.7193	0.6911	0.5923	0.5923
RSSE	1219.11	3282.26	1660.81	1400.40	896.27

3.4.1. Non-linear plots of the kinetics models

The non-linear regression plots of the kinetics models of adsorption of TOC onto FMWCNTs were obtained using OriginPro 9.1. The non-linear plots were depicted on Fig. 11 and the estimated parameters were presented in Table 6. The results revealed that pseudo-first-order kinetics model best described the adsorption of TOC onto FMWCNTs based on the non-linear regression plots as shown by the highest R^2 value and lowest RSSE in contradiction with what was obtained from the linear plots of the kinetics data. Similar observation was made by Nthunya *et al*, [66]. In addition, the predicted q_e which was calculated directly from the non-linear regression was in good agreement with the experimental q_e and showed a good approximation compared to q_e estimated from the linear model, suggesting further that the adsorption of TOC followed pseudo-first-order kinetics model. Similar results have been observed by López-Luna*et al* [70] for arsenic removal by manganese ferrite nano particles. Non-linear plots demonstrated that the goodness-of –fit of the kinetics data to Elovic and intra-particle diffusion models based on the R^2 and RSSE was consistent with the linear method but the estimated parameters were considerably high compared with that of the linear method. This observation may be due to the problems associated with the transformation of the non-linear to linear model which present a significant problem in estimating kinetics parameters, violate the fundamental theories of isotherms model and alters the error structure [65, 70, 71].

3.5. Adsorption isotherms studies

Adsorption isotherms are very vital for describing the interaction between the adsorbate and the adsorbent at equilibrium; analyzing of the equilibrium data by fitting them to the appropriate equilibrium curve is used to establish the suitable model that can be used to optimize the design of the adsorption system [49]. Linear and non-linear plots of Langmuir, Freundlich, and Harkins-Jura depicted in Fig. 12 and 13 (supplementary material) and the goodness-of-fit of the isotherms were accessed by R^2 and RSSE. Table 7 showed the parameters estimated from both linear and non-linear plots of isotherms data. As shown in Table 7, the R^2 values were generally low for Langmuir and Freundlich isotherm models which indicated that the equilibrium data were poorly fitted to these models, even though the RSSE was low. Also, adsorption parameters estimated indicated that the q_e values obtained for the Langmuir isotherm from both linear (179.21 mg/g) and non-linear (163.4 mg/g) were lower than that of the experimental (256.9 mg/g) and the R_L was less than one which further demonstrated that the equilibrium data did not follow Langmuir isotherm . The value of K_f for Freundlich was found to be 49.9 mg/g for linear and 123 8 mg/g for non-linear regression. Also, 1/n was found to be greater than unity in both cases, implying a co-operative sorption process. The results revealed a significant improvement of R^2 value and RSSE for the Harkins-Jura model indicating a better correlation and suggested multilayer adsorption process which could be explained by the existence of heterogeneous pore distribution on the surface of FMWCNTs nano-adsorbent [72].

3.6. Comparison of equilibrium adsorption capacity

The adsorption capacities of some other adsorbents in comparison with FMWCNTs used in the removal of TOC were presented in Table 8. The FMWCNTs nano-adsorbent showed a very high adsorption capacity compared to the other materials found in the literature. Though, some materials exhibited higher adsorption capacity for TOC removal, however, it is evident from Table 8 that FMWCNTs adsorbent exhibited superior performance for TOC as small quantity (20 mg) of FMWCNTs adsorbent was required to achieve adsorption capacity of 259 mg/g, demonstrating their efficiency and effectiveness as a potential adsorbent for TOC sequestration from wastewater.

3.7. Adsorption thermodynamics

The temperature was investigated in the range of 303–323K to predict the possible influence of thermodynamic parameters, such as Gibb's free energy change ΔG (kJ/mol), enthalpy change ΔH (kJ/mol), and entropy change ΔS (kJ/molK) on the adsorption of TOC onto FMWCNTs nano-adsorbent. The Gibb's free energy change (ΔG) was estimated from Eq. (21)

$$\Delta G = -RTlnK_{Te} \tag{21}$$

Table 6. Rate parameters for uptake of TOC at various doses of adsorbent and 303 K.

Non-linear Kinetic model	Dosage				
	0.02g	0.04g	0.06g	0.08g	0.1g
q_e experimental (mg/g)	259.85	130.93	88.45	69.37	55.50
Pseudo-first-order					
k_1 (min^{-1})	0.15974	0.17299	0.20644	0.65337	0.65565
q_e (mg/g)	259.92	130.76	88.18154	69.36093	55.4886
R^2	0.99998	0.9992	0.99985	1	1
RSSE	2.5651	2.50724	1.97459	7.16868×10^{-4}	4.56266×10^{-4}
Pseudo-second-order					
k_2 (min^{-1})	0.00207	0.00394	0.00728	0.75204	0.94268
q_e (mg/g)	269.97	136.378	91.4788	69.39867	55.51896
R^2	0.99985	0.99979	0.99984	1	1
RSSE	21.416	6.84116	2.1147	2.0204×10^{-4}	1.28756×10^{-4}
Elovic					
A	0.04249	0.09549	0.18448	1.49214	1.87518
B	32739	62619.84593	1.47465×10^{6}	1.93443×10^{43}	2.68026×10^{43}
R^2	0.99544	0.99645	0.99793	0.99976	0.99976
RSSE	209.48238	41.48148	11.11332	0.82241	0.52049
Intraparticle diffusion					
k_{int} (min^{-1})	41.42228	20.92374	14.20556	11.12577	8.90063
C_{int} (mg/g)	4.04211×10^{-9}	4.62641×10^{-9}	5.63906×10^{-9}	1.01812	1.01822
R^2	0.62822	0.60596	0.56507	0.4249	0.42489
RSSE	17081	4608.3899	2338.78032	1975.33515	1264.23332

Table 7. Adsorption isotherms parameter estimation.

Isotherms	Linear	Nonlinear
Langmuir		
q_o (mgg^{-1})	179.215	163.411
R_L	14	16.90217
R^2	0.57964	0.2288
RSSE	7.57022×10^{-5}	15848.38317
Freundlich		
k_f	49.94	123.82832
N	11	0.25292
R^2	0.23815	0.32261
RSSE	3.61978	13916.94196
Harkins-Jura		
A_H	-7367.03	1615.2432
B_H	-0.9733	0.57598
R^2	0.90014	0.88775
RSSE	4.24941×10^{-9}	2716.96891

Table 8. Comparison of FMWCNTs Nano-adsorbent to the other materials on the adsorption of TOC.

Adsorbent	Dosage (mg)	Maximum adsorption capacity (mg/g)	Reference
FMWCNTs	20	259.6	The current work
Chitosan (CS)	50–200	51	[73]
Chitosan-O-arginine	50–200	40	[73]
Granular AC	0–7500	1850	[74]
Granular AC	2000	164.05	[75]

Where R is the gas constant (8.314J/(molK), T is the absolute temperature and K_{Te} is the thermodynamics equilibrium constant and it is presented as:

$$K_{Te} = \frac{C_{ad}}{C_e} \tag{22}$$

Where C_e (mg/L) represent the equilibrium concentration of TOC in solution and C_{ad} (mg/L) the concentration of TOC on the adsorbent at equilibrium. The values ΔH and ΔS were estimated from the following Van'T Hoff Equation

$$\ln K_{Te} = \frac{\Delta S}{R} - \frac{1}{T}\left(\frac{\Delta H}{R}\right) \tag{23}$$

The values of ΔH and ΔS were estimated from the slope and intercept of the plot of lnK_{Te} versus $\frac{1}{T}$ as shown in Fig. 14 (Supplementary). Thermodynamic parameters for the adsorption of TOC from produced water using FMWCNTs were presented in Table 9.

The negative values of ΔG indicated the feasibility and spontaneity of the adsorption process. The decrease in the negativity of ΔG with increase in temperature for the adsorption of TOC onto FMWCNTs nano-adsorbent suggested the exothermic nature of the adsorption process. The negative value of ΔH affirmed the exothermic nature of adsorption of TOC onto FMWCNTs nano-adsorbent and this implied that the adsorption process is feasible at low temperature [76]. It was found that the value of ΔS was negative for the TOC adsorption process; the negative values of ΔS indicated a reduction in randomness at the solid/liquid interface during adsorption process of TOC on the FMWCNTs nano-adsorbent [77].

4. Conclusion

This study demonstrated that TOC could be removed from crude oil-produced water using PMWCNTs and FMWCNTs. The FMWCNTs exhibited better performance probably due to the incorporation of the PSE molecule which enhanced the hydrophilic properties of the MWCNTs, improved their wettability and enhanced their adsorption capability in the removal of TOC. The adsorption capacity was found to be affected by solution temperature, contact time and adsorbent dosage. The CCD of RSM employed for the optimization of process parameters revealed the predicted optimum operating condition of; contact time (49.70 min), solution temperature (34.81 °C) and adsorbent dosage (0.02 g). Adsorption of TOC was better described by Harkins-Jura isotherm and pseudo-first-order kinetic models. The thermodynamics study confirmed that the sorption process is spontaneous, feasible and exothermic as ΔG and ΔH were negative. The negative entropy change (ΔS) revealed a reduction in randomness due to increased stability of TOC on the nano-adsorbent surface and the inference drawn from this is that less energy of interaction between the of adsorbate and the adsorbent is required. The results obtained from this study demonstrated that FMWCNTs may be explored as a promising nano-adsorbent for removal of TOC from crude oil-produce water. Future study should be tailored towards performance evaluation of the FMWCNTs using wastewater from other sources. Research should be focused on regeneration/reusability study and column studies for a better understanding of the adsorption mechanism to designing a viable procedure for practical application.

Table 9. Thermodynamic parameters for TOC adsorption onto nano-adsorbent.

Sorbate	Temperature (K)	K_{Te}	ΔG (kJ/mol)	ΔH (kJ/mol)	ΔS (kJ/molK)	R^2
TOC	303	1.57×10^3	-16.6991			
	313	1.06×10^3	-15.8082	-19.9436	-0.0050	0.9006
	323	9.63×10^2	-15.5933			

Declarations

Author contribution statement

ADEWOYE, T. L.: Performed the experiments; Analyzed and interpreted the data; Wrote the paper.

OGUNLEYE, O. O., ABDULKAREEM A. S. & SALAWUDEEN T. O.: Conceived and designed the experiments; Contributed reagents, materials, analysis tools or data; Wrote the paper.

Tijani J. O.: Analyzed and interpreted the data; Wrote the paper.

Funding statement

This research did not receive any specific grant from funding agencies in the public, commercial, or not-for-profit sectors.

Data availability statement

Data included in article/supp. material/referenced in article.

Declaration of interests statement

The authors declare no conflict of interest.

Additional information

Supplementary content related to this article has been published online at https://doi.org/10.1016/j.heliyon.2020.e05866.

References

[1] K. Sam, N. Zabbey, Contaminated land and wetland remediation in Nigeria: opportunities for sustainable livelihood creation, Sci. Total Environ. 639 (2018) 1560–1573.
[2] E.S. Osuagwu, E. Olaifa, Effects of oil spills on fish production in the Niger Delta, PloS One 13 (2018), e0205114.
[3] N. Udeh, I. Nwaogazie, Y. Momoh, Bio-remediation of a crude oil contaminated soil using water hyacinth (Eichhornia crassipes), Adv. Appl. Sci. Res. 4 (2013) 362–369.
[4] A. Bruederle, R. Hodler, Effect of oil spills on infant mortality in Nigeria, Proc. Natl. Acad. Sci. Unit. States Am. 116 (2019) 5467–5471.
[5] Sikoki F. BabatundeB, G. Avwiri, Y. Chad-Umoreh, Review of the status of radioactivity profile in the oil and gas producing areas of the Niger delta region of Nigeria, J. Environ. Radioact. 202 (2019) 66–73.
[6] T. Afzal, M.H. Isa, M.R. ul Mustafa, Removal of organic pollutants from produced water using Fenton oxidation, in: E3S Web of Conferences, EDP Sciences, 2018.
[7] M.C. Onojake, U.I. Abanum, Evaluation and management of produced water from selected oil fields in Niger Delta, Nigeria, Arch. Appl. Sci. Res. 4 (1) (2012) 39–47.
[8] T. Nonato, A. De A Alves, M. Sens, D. RL, Produced water from oil - a review of the main treatment technologies, J. Environ. Chem. Toxicol. 2 (1) (2018) 23–27.
[9] A.K. Gazali, A.N. Alkali, Y. Mohammed, D. Yaba, D.D. Mohammed, M. Kodomi, Environmental impact of produced water and drilling waste discharge fromthe Niger Delta petroleum industry, IOSR J. Eng. 7 (2017) 22–29.
[10] H. Zhu, T. Chen, J. Liu, D. Li, Adsorption of tetracycline antibiotics from an aqueous solution onto graphene oxide/calcium alginate composite fibers, RSC Adv. 8 (2018) 2616–2621.
[11] EPA, Parameter of Water Quality: Interpretation and Standard, Environmental Protection Agency, Ireland, 2001.
[12] E.T. Igunnu, G.Z. Chen, Produced water treament technologies, Int. J. Low Carbon Technol. 9 (3) (2014) 157–177.
[13] H. Rawindran, S. Krishnan, C. Sinnathambi, A review on overboard CEOR discarged produced water treatment and remediation, IOP Conf. Series: Mater. Eng. 206 (2017) 1–8.
[14] R.T. Duraisamy, A.H. Beni, A. Henni, State of the art treatment of produced water, in: W. Elshorbagy, R.K. Chowdhury (Eds.), Water Treatment, InTech, London, 2013, pp. 119–222.
[15] M. Bankole, A. Abdulkareem, J. Tijani, S. Ochigbo, A. Afolabi, And W. Roos, Chemical oxygen demand removal from electroplating wastewater by purified and polymer functionalized carbon nanotubes adsorbents, Water Res. Industry 18 (2017) 33–50.
[16] M. Fathy, M. El-Sayed, M. Ramzi, O. Abdelraheem, Adsorption separation of condensate oil from produced water using ACTF prepared of oil palm leaves by batch and fixed bed techniques, Egypt. J. Petrol. 27 (2018) 319–326.
[17] V.K. Gupta, I. Ali, T. Saleh, A. Nayak, S. Agarwal, Chemical treatment technologies for waste-water recycling- an overview, Royal Society of Chemistry 2012 (2) (2012) 6380–6388.
[18] A. Inyinbor, F. Adekola, G.A. Olatunji, Kinetics, isotherms and thermodynamic modeling of liquid phase adsorption of Rhodamine B dye onto Raphia hookerie fruit epicarp, Water Res. Industry 15 (2016) 14–27.
[19] L. Chan, W. Cheung, S. Allen, G. McKay, Error analysis of adsorption isotherm models for acid dyes onto bamboo derived activated carbon, Chin. J. Chem. Eng. 20 (3) (2012) 535–542.
[20] D. Balarak, F.K. Mostafapour, Akbari, A. Joghtaei, Adsorption of amoxicillin antibiotic from pharmaceutical wastewater by activated carbon prepared from Azolla filiculoides, J. Pharmaceutical Res. Int. (2017) 1–13.
[21] R. Das, S.B.A. Hamid, M.E. Ali, A.F. Ismail, M. Annuar, S. Ramakrishna, Multifunctional carbon nanotubes in water treatment: the present, past and future, Desalination 354 (2014) 160–179.
[22] M. Bankole, J.O. Tijani, I. Mohammed, A. Abdulkareem, A review on nanotechnology as a tool of change in Nigeria, Sci. Res. Essays 9 (2014) 213–223.
[23] A. Osikoya, D. Wankasi, R. Vala, A. Afolabi, E. Dikio, Synthesis, Characterization and adsorption studies of fluorine–doped carbon nanotubes, Dig. J. Nanomater. Bios. 9 (2014) 1187–1197.
[24] N. Mubarak, J. Sahu, E. Abdullah, N. Jayakumar, Removal of heavy metals from wastewater using carbon nanotubes, Separ. Purif. Rev. 43 (2014) 311–338.
[25] E.F. Mohamed, G. Awad, C. Andriantsiferana, H. Delmas, Effect of Salinity and PH on the industrial effluent treatment by activated carbon: modeling of the kinetic adsorption and equilibrium isotherms, Environ. Manag. Sustain. Dev. 8 (2019) 77–94.
[26] V.K. Upadhyayula, S. Deng, M.C. Mitchell, G.B. Smith, Application of carbon nanotube technology for removal of contaminants in drinking water: a review, Sci. Total Environ., 408 (2009) 1–13.
[27] S. Parlayici, V. Eskizeybek, A. Avcı, E. Pehlivan, Removal of chromium (VI) using activated carbon-supported-functionalized carbon nanotubes, J. Nanostructure Chem. 5 (2015) 255–263.
[28] F.D. Guerra, M.F. Attia, D.C. Whitehead, F. Alexis, Nanotechnology for environmental remediation: materials and applications, Molecules 23 (2018) 1760.
[29] S.-Y. Wang, H.-M. Wu, Specificity bio-identification of CNT-based transistor, in: Journal of Physics: Conference Series, IOP Publishing, 2017.
[30] R.J. Chen, Y. Zhang, D. Wang, H. Dai, Noncovalent sidewall functionalization of single-walled carbon nanotubes for protein immobilization, J. Am. Chem. Soc. 123 (2001) 3838–3839.
[31] L.N. Nthunya, KhumaloNP, A.R. Verliefde, B.B. Mamba, D. MhlangaS, Quantitative analysis of phenols and PAHs in the Nandoni Dam in Limpopo Province, South Africa: a preliminary study for dam water quality management, Phys. Chem. Earth, Parts A/B/C 112 (2019a) 228–236.
[32] E. Lember, K. Pachel, E. Loigu, Removal of heavy metals and total organic carbon from wastewater using powdered activated carbon, Proc. Est. Acad. Sci. 68 (1) (2019).
[33] M. Bankole, I. Mohammed, A. Abdulkareem, J. Tijani, S. Ochigbo, O. Abubakre, AfolabiA, Optimization of supported bimetallic (Fe-Co/CaCO3) catalyst synthesis parameters for carbon nanotubes growth using factorial experimental design, J. Alloys Compd. 749 (2018) 85–102.
[34] Farghali A. BahgatM, W. El Rouby, M. Khedr, Synthesis and modification of multi-walled carbon nano-tubes (MWCNTs) for water treatment applications, J. Anal. Appl. Pyrol. 92 (2011) 307–313.
[35] A. Mane, R. Pardeshi, V. Gore, R. Walave, S. Manjrekar, G. Sutar, Water quality and sediment analysis at selected locations of Pavana river of Pune district, Maharashtra, J. Chem. Pharmaceut. Res. 5 (8) (2013) 91–102.
[36] S. Lagergren, Zur theorie der sogenannten adsorption geloster stoffe, 1898.
[37] G. McKay, Y. Ho, Pseudo-second order model for sorption processes, Process Biochem. 34 (5) (1999) 451–465.
[38] P.-X. Hou, C. Liu, H.-M. Cheng, Purification of carbon nanotubes, Carbon 46 (2008) 2003–2025.
[39] Y.-h Shih, M.-s Li, Adsorption of selected volatile organic vapors on multiwall carbon nanotubes, J. Hazard Mater. 154 (1-3) (2008) 21–28.
[40] K. Zare, V.K. Gupta, O. Moradi, A.S.H. Makhlouf, M. Sillanpää, M.N. Nadagouda, H. Sadegh, R. Shahryari-ghoshekandi, A. Pal, Z.-j. Wang, I. Tyagi, M. Kazemi, A comparative study on the basis of adsorption capacity between CNTs and activated carbon as adsorbents for removal of noxious synthetic dyes: a review, J. Nanostruct. Chem. 5 (2) (2015) 227–236.
[41] A.I. Yardimci, S. Yılmaz, Y. Selamet, The effects of catalyst pretreatment, growth atmosphere and temperature on carbon nanotube synthesis using Co–Mo/MgO catalyst, Diam. Relat. Mater. 60 (2015) 81–86.
[42] K. Balasubramanian, M. Burghard, Chemically functionalized carbon nanotubes, Small 1 (2) (2005) 180–192.
[43] H. Murphy, P. Papakonstantinou, T.T. Okpalugo, Raman study of multiwalled carbon nanotubes functionalized with oxygen groups, J. Vac. Sci. Technol. B: Microelectronics and Nanometer Structures Processing, Measurement, and Phenomena 24 (2) (2006) 715–720.
[44] M. Dresselhaus, A. Jorio, A. Souza Filho, R. Saito, Defect characterization in graphene and carbon nanotubes using Raman spectroscopy, Phil. Trans. Math. Phys. Eng. Sci. 368 (1932) (2010) 5355–5377.
[45] Y. Xie, J. Zhao, L. Zhanggao, et al., Preparation and electromagnetic properties of chitosan-decorated ferrite-filled multi-walled carbon nanotubes/polythiophene composites, Compos. Sci. Technol. 99 (2014) 141–146.
[46] Z. Mitróová, N. Tomašovičová, G. Lancz, J. Kováč, I. Vávra, P. Kopčanský, Preparation and Characterization of Carbon Nanotubes Functionalized by Magnetite Nanoparticles. Olomouc, Czech Republic, EU 10 (2010) 12–14.
[47] S. Hussain, p Jha, R. Chouksey, et al., Spectroscopic investigation of modified single wall carbon nanotube (SWCNT), J. Mod. Phys 2 (2011) 538–543.

[48] K.A. Wepasnick, B.A. Smith, J.L. Bitter, D.H. Fairbrother, Chemical and structural characterization of carbon nanotube surfaces, Anal. Bioanal. Chem. 396 (2010) 1003–1014.
[49] G. Crini, E. Lichtfouse, WilsonLD, Morin-CriniN, Adsorption-oriented Processes Using Conventional and Non-conventional Adsorbents for Wastewater Treatment Green Adsorbents for Pollutant Removal, Springer, 2018, pp. 23–71.
[50] R. Baby, HusseinMZ. saifullahB, Carbon nanomaterials for the treatment of heavy metal-contaminated water and environmental remediation, Nanoscale Res. Lett. 14 (1) (2019) 341.
[51] W.A. Hamzat, A.S. Abdulkareem, M.T. Bankole, J.O. Tijani, A.S. Kovo, O.K. Abubakre, Adsorption studies on the treatment of battery wastewater by purified carbon nanotubes (P-CNTs) and polyethylene glycol carbon nanotubes (PEG-CNTs), J. Environ. Sci. Health A54 (2019) 827–839.
[52] F. Su, C. Lu, S. Hu, Adsorption of benzene, toluene, ethylbenzene and p-xylene by NaOCl-oxidized carbon nanotubes, Colloid. Surface. Physicochem. Eng. Aspect. 353 (2010) 83–91.
[53] H. Kalavathy, B. Karthik, L.R. Miranda, Removal and recovery of Ni and Zn from aqueous solution using activated carbon from Hevea brasiliensis: batch and column studies, Colloids Surf. B Biointerfaces 78 (2) (2010) 291–302.
[54] W. Fan, R. Zhang, Structural and electronic properties of single-walled carbon nanotubes adsorbed with 1-pyrenebutanoic acid, succinimidyl ester, Sci. China, Ser. B: Chemistry 51 (12) (2008) 1203–1210.
[55] M.A. Salam, Removal of heavy metal ions from aqueous solutions with multi-walled carbon nanotubes: kinetic and thermodynamic studies, Int. J. Environ. Sci. Technol. 10 (4) (2013) 677–688.
[56] A.A. Oladipo, O.J. Adeleye, A.S. Oladipo, A.O. Aleshinloye, Bio-derived MgO nanopowders for BOD and COD reduction from tannery wastewater, J. Water Process Eng. 16 (2017) 142–148.
[57] O.S. Ayanda, O.S. Fatoki, F.A. Adekola, B.J. Ximba, Removal of tributyltin from shipyard process wastewater by fly ash, activated carbon and fly ash/activated carbon composite: adsorption models and kinetics, J. Chem. Technol. Biotechnol. 88 (12) (2013) 2201–2208.
[58] N.N. Desai, V.S. Soraganvi, V.K. Madabhavi, Solar photocatalytic degradation of organic contaminants in landfill leachate using TiO 2 nanoparticles by RSM and ANN, Nat. Environ. Pollut. Technol. 19 (2) (2020).
[59] V. Kozik, K. Barbusinski, M. Thomas, A. Sroda, J. Jampilek, A. Sochanik, A. Bak, Taguchi method and response surface methodology in the treatment of highly contaminated tannery wastewater using commercial potassium ferrate, Materials 12 (22) (2019) 3784.
[60] A. Fegousse, A. El Gaidoumi, Y. Miyah, R. El Mountassir, A. Lahrichi, Pineapple bark performance in dyes adsorption: optimization by the central composite design, J. Chem. (2019).
[61] S.O. Egbuna, C.N. Mbah, J.O. Okoye, Optimal process parameters for the adsorption of methylene blue on thermally activated enugu white clay as A local adsorbent, Int. J. Eng. Sci. Invention 4 (9) (2015) 32–42.
[62] J. Neff, K. Lee, E.M. DeBlois, Produced Water: Overview of Composition, Fates, and Effects Produced Water, Springer, 2011, pp. 3–54.
[63] BakkeT, J. Klungsøyr, S. Sanni, Environmental impacts of produced water and drilling waste discharges from the Norwegian offshore petroleum industry, Mar. Environ. Res. 92 (2013) 154–169.
[64] NIS, *Nigerian Standard for Drinking Water Quality* Standard Organization of Nigerial, 2007.
[65] E.E. Jasper, OnwukaJC. AjibolaVO, Nonlinear regression analysis of the sorption of crystal violet and methylene blue from aqueous solutions onto an agro-waste derived activated carbon, Appl. Water Sci. 10 (6) (2020) 1–11.
[66] L.N. Nthunya, L. Gutierrez, S. Derese, B.B. Mamba, A.R. Verliefde, S.D. Mhlanga, Adsorption of phenolic compounds by polyacrylonitrile nanofibre membranes: a pretreatment for the removal of hydrophobic bearing compounds from water, J. Environ. Chem. Eng. 7 (4) (2019b) 103254.
[67] C.B. Vidal, A.L. Barros, C.P. Mouro, et al., Adsorption of polycyclic aromatic hydrocarbons from aqueous solutions by modified periodic mesoporous organosilica, J. Colloid Interface Sci. 357 (2011) 466–473.
[68] M. Abdelkreem, Adsorption of phenol from industrial wastewater using olive mill waste, APCBEE Proc. 5 (2013) 349–357.
[69] M.S. Sajab, C.H. Chia, S. Zakaria, M. Sillanpää, Removal of organic pollutants and decolorization of bleaching effluents from pulp and paper mill by adsorption using chemically treated oil palm empty fruit bunch fibers, BioResources 9 (3) (2014) 4517–4527.
[70] J. López-Luna, E. Ramírez-MontesL, S. Martinez-Vargas, A.I. Martínez, O.F. Mijangos-Ricardez, A. María del Carmen, V. Vázquez-Hipólito, Linear and nonlinear kinetic and isotherm adsorption models for arsenic removal by manganese ferrite nanoparticles, SN Appl. Sci. 1 (8) (2019) 950.
[71] A.E. Hamidi, S. Arsalane, M. Halim, Kinetics and isotherm studies of copper removal by brushite calcium phosphate: linear and non-linear regression comparison, E-J. Chem. 9 (3) (2012) 1532–1542. http://www.ejchem.net.
[72] N. Ayawei, A.N. Ebelegi, D. Wankasi, Modelling and interpretation of adsorption isotherms, J. Chem. 2017 (2017).
[73] H.H. Hefni, M. Nagy, M.M. Azab, HusseinMH, O-Acylation of chitosan by l-arginine to remove the heavy metals and total organic carbon (TOC) from wastewater, Egypt. J. Petrol. 29 (1) (2020) 31–38.
[74] S. Ghafoori, K.K. Shah, M. Mehrvar, P.K. Chan, Pharmaceutical wastewater treatment using granular activated carbon and UV/H2O2 processes: experimental analysis and modelling, Can. J. Chem. Eng. 92 (7) (2014) 1163–1173.
[75] F. Ademiluyi, S. Amadi, N.J. Amakama, Adsorption and treatment of organic contaminants using activated carbon from waste Nigerian bamboo, J. Appl. Sci. Environ. Manag. 13 (3) (2009).
[76] K.M. Doke, E.M. Khan, Adsorption thermodynamics to clean up wastewater; critical review, Rev. Environ. Sci. Biotechnol. 12 (1) (2013) 25–44.
[77] A. Ofomaja, E. Unuabonah, N. Oladoja, Competitive modeling for the biosorptive removal of copper and lead ions from aqueous solution by Mansonia wood sawdust, Biores. Technol. 101 (11) (2010) 3844–3852.